Check for updates

Original Research

Advances in Structural Engineering

Advances in Structural Engineering
1–17
© The Author(s) 2020
Article reuse guidelines:
sagepub.com/journals-permissions
DOI: 10.1177/1369433220958763
journals.sagepub.com/home/ase
SAGE

Aerodynamic coefficients and pressure distribution on two circular cylinders with free end immersed in experimentally produced downburst-like outflows

Djordje Romanic[1,2,3], Andrea Ballestracci[1], Federico Canepa[1], Giovanni Solari[1] and Horia Hangan[2]

Abstract

Thunderstorms winds are localized and transient phenomena characterized by three-dimensional non-stationary velocity fields. While numerous studies investigated the wind loading on cantilevered structures under thunderstorm downburst winds, there is a lack of fundamental research on the behavior of simple circular cylinders subjected to downburst-like outflows. This paper investigates the pressure distribution and aerodynamic coefficients of two cylinders with different diameters immersed in three different types of wind: (1) isolated downburst (DB); (2) downburst embedded in an atmospheric boundary layer (ABL) wind (DBABL); and (3) steady ABL wind. The focus of this study is to provide a comparative analysis between aerodynamic coefficients (drag and lift) and surface pressures that result from these three different wind systems. The ABL winds caused a higher drag on the thinner cylinder than the two DB-like outflows. The lift coefficients during the primary vortex passage in the DB-like outflows were negative at the base of the cylinders and approached zero or to slightly positive values close to the cylinders' top. The location of the cylinders in DB-like outflows is the dominant factor for their aerodynamics.

Keywords

downbursts, circular cylinders, aerodynamic coefficients, drag, lift, surface pressures, turbulent flows, wind engineering

Introduction

On-going research over the last several decades has demonstrated that the wind loading caused by the atmospheric boundary layer (ABL) winds profoundly differs from the wind loading due to highly three-dimensional and transient winds, such as thunderstorm downbursts (Hangan et al., 2019; Solari, 2016). The main differences in the structural behavior to different wind systems are not only due to potentially higher wind speeds in downburst outflows but predominantly are due to different vertical profiles of the mean wind speed and turbulent characteristics between the two flows, as well as different velocity distributions (De Gaetano et al., 2014; Hangan et al., 2019). By definition, thunderstorm downbursts are cold downdrafts that originate from a cumulonimbus cloud and spread radially upon hitting the surface. The main contributors to the negative buoyancy of descending downdrafts are evaporation and, to a smaller extent, melting of hydrometeors inside and below the cloud, as well as the drag due to the falling hydrometeors (e.g. falling raindrops, ice, and graupel). Other contributing factors for descending currents in supercell cumulonimbus clouds have also been identified and discussed in the literature (Markowski, 2002).

In wind engineering applications, circular cylinders are found in construction designs of lighting and

[1]Department of Civil, Chemical and Environmental Engineering, Polytechnic School, University of Genoa, Genoa, Italy
[2]Wind Engineering, Energy and Environment Research Institute, Western University, London, ON, Canada
[3]Department of Atmospheric and Oceanic Sciences, McGill University, Montréal, QC, Canada

Corresponding author:
Djordje Romanic, Wind Engineering, Energy and Environment Research Institute, Western University, 2535 Advanced Avenue, London, ON N6M 0E2, Canada.
Email: dromanic@uwo.ca

luminary poles, chimneys and antenna masts, power transmission lines, silos, wind turbine towers, and bridge supports and cranes, to name few applications. Therefore, the proper understanding of aerodynamic wind coefficients and surface pressures on circular cylinders is needed for the appropriate design of cylindrical structures. While these parameters are well researched and properly reported in many international wind building codes for the case of ABL winds, there is a lack of fundamental research on the behavior of circular cylinders under the transient and non-Gaussian wind actions of downburst-like outflows.

When it comes to cantilevered structures, a lot of wind engineering research has recently been focused on the structural behavior of transmission lines and towers under downburst winds. Savory et al. (2001) performed dynamic structural analysis of a lattice transmission tower to investigate wind loading and failure criteria due to downbursts and tornadoes. Their study concluded that the calculated tornado failures have better agreement with the field damage surveys. However, the study neglected vertical downburst wind components, as well as downburst forces on conductors. Later, Shehata et al. (2005) and Shehata and Damatty (2007) investigated the responses of transmission lines under downburst wind using a computational fluid dynamics (CFD) tool. More recently, Wang et al. (2009), Darwish et al. (2010), Darwish and Damatty (2011), Qu et al. (2013), and Elawady et al. (2017, 2018) studied transmission line responses under different downburst-like outflows by considering different structural properties of transmission lines. Ibrahim et al. (2017) showed that downbursts could be more hazardous for pre-stressed concrete poles than tornadoes.

In a study on thunderstorm response spectrum technique, Solari (2016) discussed the need for more research on comparative analyses between ABL and thunderstorm winds. One such study was carried out earlier by Kim et al. (2007), in which the authors examined the differences between ABL and downburst wind loads on tall buildings. They showed that the large downdrafts can produce higher shear forces and base moments than the ABL winds. Chen and Letchford (2004) simulated downburst wind actions on a cantilevered structure by assuming deterministic mean wind speed and stochastic fluctuations. They demonstrated that the structure was highly sensitive to wind fluctuations and the properties of coherence function. Later, Chay et al. (2006) concluded that lower turbulence intensities and higher mean wind speeds produced in a downburst outflow than in an ABL wind results in a higher and more correlated loading on a long span structure. In two consecutive papers, Nguyen et al. (2015a, 2015b) investigated aeroelastic responses of complex lighting poles and antenna masts subjected to ABL winds. The obtained aerodynamic coefficients were analyzed in the context of quasi-steady theory. Their analyses based on sectional model tests demonstrated the existence of certain configurations prone to wind instabilities and strong dynamic responses. Recently, Hangan et al. (2019) discussed the applicability of quasi-steady theory for non-synoptic winds such as downbursts and tornados. However, no study experimentally investigated the influence of downburst-like outflows on slender circular cylinders, which are among the most significant structural shapes in the field of wind engineering.

The main goal of this paper is to investigate experimentally the pressure distribution and associated aerodynamic force coefficients for two circular cylinders of different diameters with a free end that are immersed in downburst-like outflows. While the model geometry is rather simple, the investigated flows are complex and not investigated thus far in terms of the proposed application. The two circular cylinders were subjected to: (1) An isolated downburst outflow produced without ABL winds; (2) a downburst outflow embedded in ABL winds; and (3) the control case of ABL winds without any downburst outflow.

Experiments setup and methodology

The WindEEE Dome and experiments setup

All physical experiments in this study were performed in the WindEEE Dome (Hangan et al., 2017), which is a large-scale wind simulator capable of producing downburst-like outflows at different geometric scales varying from approximately 1:100 to over 1:1000 (Junayed et al., 2019; Romanic et al., 2019b). The velocity scales are typically between 1:1 and 1:4. This unique wind simulator is capable of simultaneously producing different ABL winds and downburst outflows (Romanic et al., 2019a) (Figure 1).

Downburst-like outflows in the WindEEE Dome are created by closing the louvers on the bell mouth and pressurizing the upper plenum (Figure 1(b)). The pressurization is achieved by using six large fans situated in the upper plenum, each fan with a diameter of 2 m. When the upper chamber is pressurized, the sudden opening of louvers creates an impinging jet that spreads out horizontally upon hitting the surface of the test chamber. The use of impinging jets to replicate downburst-like outflows was proposed by Hjelmfelt (1988) after demonstrating that these two flows have similar radial velocity profiles. The simultaneous downburst and ABL wind mode of the WindEEE Dome are similar to the isolated downburst mode, with the exception that the impinging jet is released

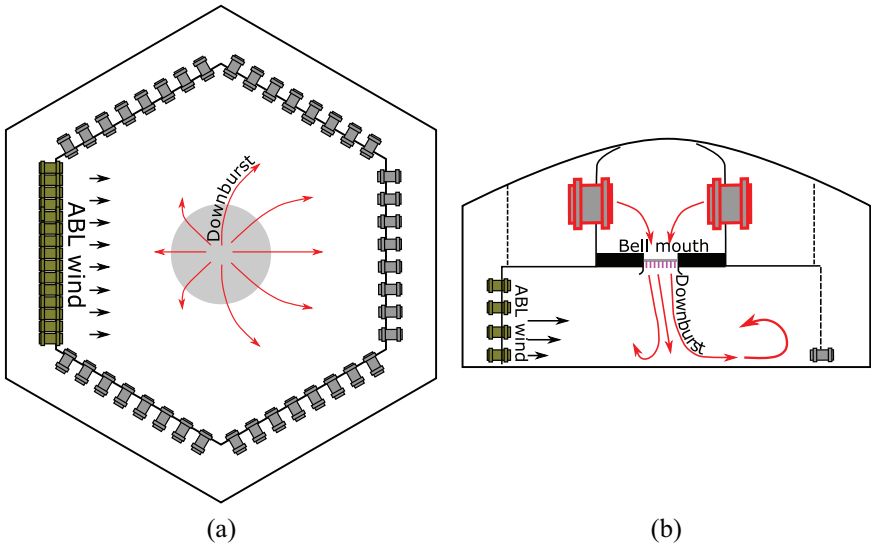

Figure 1. Downburst released in the background ABL winds inside the WindEEE Dome from (a) top-view and (b) side-view perspectives.

into an already developed ABL wind (Figure 1). Nine different momentum ratios of ABL winds and downburst impinging jets were recently investigated in Romanic et al. (2019a). The ABL winds were generated by using 60 fans installed on one of six peripheral walls in the test chamber (Figure 1(a)). The 60-fan wall contains four rows of 15 fans per row. A detailed description of the WindEEE Dome capabilities and a comparison of generated ABL winds against the Engineering Sciences Data Unit (ESDU) wind and turbulence intensity profiles (ESDU, 2002) are presented in Hangan et al. (2017) and Jubayer et al. (2019).

Hereafter, the isolated downburst-like outflow and the downburst simultaneously combined with ABL winds are referred to as DB and DBABL, respectively. The jet centerline velocity at the bell mouth level in the DB and DBABL downdrafts were 12.3 and 11.8 m s^{-1}, respectively, whereas the ABL wind velocity at the height of the cylinder was 3.3 m s^{-1}. The selected configuration of two flows was chosen due to the minimal loss of jet momentum between DB and DBABL cases in this closed-circuit mode of the WindEEE Dome (Romanic et al., 2019a). All investigated downbursts had a diameter of $D = 3.2$ m and the height of the test chamber was $H = 3.8$ m.

The diameters of two rigid Plexiglas circular cylinders considered in this study were $d_1 = 4$ mm and $d_2 = 12.5$ mm (Figure 2). The cylinders were instrumented with 12 pressure taps equally distributed along the cylinders' circumferences and at a distance of $10d$ from the free edge (Figure 2). The angle between two adjacent pressure taps was 30°. The rest of the setup is shown in Table 1 and Figure 2. Since each cylinder was instrumented with only a single row of pressure taps, the different height of cylinders was simulated by increasing the cylinders' height by raising them from

Table 1. Summary of experiments: setup and governing parameters.

Parameter	Value
Downdraft diameter, D (m)	3.2
Chamber height, H (m)	3.8
Diameter of cylinder, d (mm)	4; 12.5
Distances of cylinders from downdraft center, r (m)	1.60; 3.20; 3.84
Non-dimensional distances of cylinders from downdraft center, r/D	0.5; 1.0; 1.2
Maximum measuring height, L (cm)	90
Measuring heights, z (cm)	5; 10; 15; 20; 30; 50; 70; 90
Non-dimensional measuring heights, z/L	0.056; 0.111; 0.167; 0.222; 0.333; 0.556; 0.778; 1
Downburst duration, ΔT (s)	4
Pressure measurements sampling frequency, f_{sp} (Hz)	500
Velocity measurements sampling frequency, f_{sv} (Hz)	1250

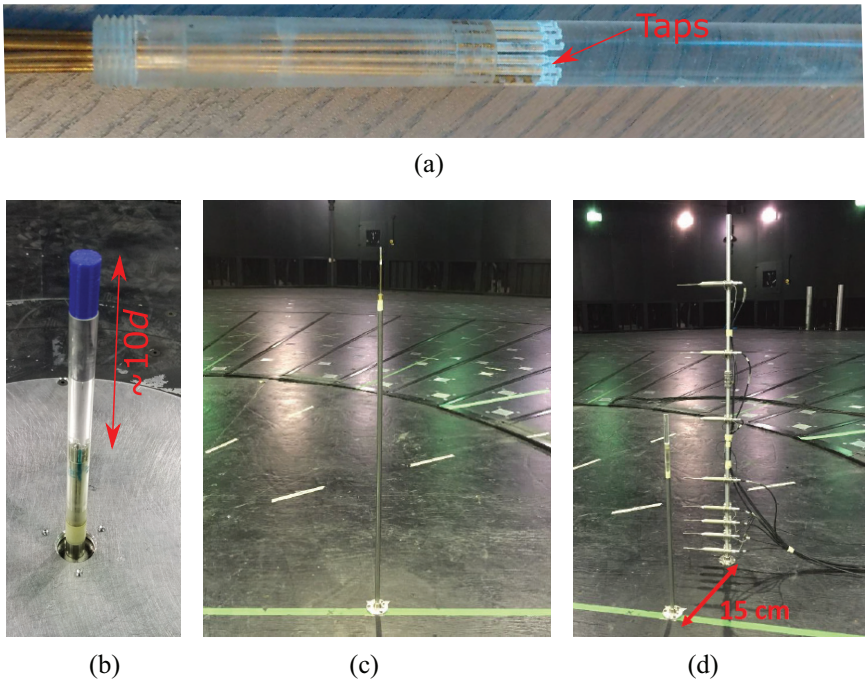

Figure 2. Two cylinders subjected to DB and DBABL outflows in the WindEEE Dome. (a) is a closer look at the pressure taps on the thinner cylinder, (b) shows the distance between the pressure taps and the free end of mounted cylinder, (c) Shows the cylinder d_1 (thinner), while other three panels show the cylinder d_2 (thicker), and (d) Also shows the Cobra probes installed on a rack.

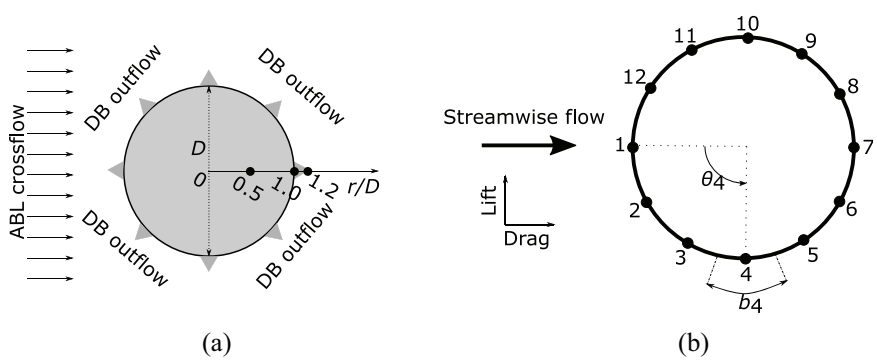

Figure 3. (a) The locations of cylinders in the outflow (black dots). The directions of ABL winds and DB outflow indicated with black arrows and gray triangles, respectively. (b) Spatial distribution of pressure taps and the direction of positive lift and drag forces to the incoming flow. The tributary length (b) and arc angle (θ) demonstrated on the example of tap #4.

the floor. The installation of multiple rows of pressure taps on these two cylinders (keeping 12 taps per row) is not feasible due to the technical challenge of limited space for pressure tubing inside the cylinders. The base support for the $d_1 = 4$ mm cylinder was a cylinder of different diameter (Figure 2(c)), but the insertion of the thicker base did not influence the result due to the separation between the taps and the base that was $>20d_1$ (Fox and West, 1993a, 1993b). In both DB and DBABL cases, r/D was measured from the touchdown position of the DB downdraft. The locations of cylinders in the DB-like outflows are shown in Figure 3(a).

The pressure measurement system used the Electronically Scanned Pressure (ESP) scanners and Digital Temperature Compensation (DTC) Initium to record differential pressure at each of 12 pressure taps. The pressure scanners are electronic pressure units that measure differential pressures with an array of silicon piezoresistive pressure sensors. All 12 pressure taps were connected to a single 32-port scanner that can

accommodate tubes with an outer diameter of 1 mm. The pressure range for the scanners was ±4 inches of water (equivalent to ±1 kPa). Proper and periodic on-line calibration of the system maintained static errors within ±0.03%. The DTC Initium is a pressure data acquisition system that was connected to the scanner via an Ethernet-based connection. The accuracy of the DTC Initium is ±0.05% over the entire operating temperature range (0°C–70°C). The mean air temperature during the tests was 21.2°C.

The velocity measurements were performed using four-hole Cobra probes. The position of eight Cobra probes on the vertical rack is shown in Figure 2(d), and their z/L heights are identical to the pressure measurement heights (Table 1). It is important to note that the velocity and pressure measurements in the present experiments were not synchronized with each other. Also, the velocity measurements were only conducted during the testing of d_2 (thicker) cylinder (Figure 2(c) and (d)) because the tested flows concerning d_1 are the same as in the case of d_2 cylinder. Cobra probes are robust instruments designed to measure turbulent flows by capturing three velocity components from a 45° cone concerning the incoming flow. The measuring accuracy of Cobra probes is within ±0.5 m s^{-1} up to approximately 30% turbulence intensity. Lastly, the velocity measurements were conducted in the same r/D locations that were used in the pressure measurements.

Methodology

The drag (c_D) and lift (c_L) coefficients were calculated as:

$$c_D = \frac{F_D}{0.5\rho d U_{ref}^2}, \tag{1}$$

$$c_L = \frac{F_L}{0.5\rho d U_{ref}^2}, \tag{2}$$

where ρ is the air density, U_{ref} is the reference velocity, and F_D and F_L are the drag and lift forces, respectively, calculated from the surface pressure measurements as:

$$F_D = \oiint_S \left(p - p_{ref}\right)_D ds, \tag{3}$$

$$F_L = \oiint_S \left(p - p_{ref}\right)_L ds. \tag{4}$$

Here, $\left(p - p_{ref}\right)_D$ and $\left(p - p_{ref}\right)_L$ are the components of differential pressures in the drag and lift directions (Figure 2(b)), respectively, p_{ref} is the reference static pressure, and ds is the unit area. Expressing the results per unit length and assigning a tributary width (b) for each pressure tap (Figure 2(b)), equations (3) and (4) read:

$$F_D = \sum_{i=1}^{12} \left(p_i - p_{ref}\right) b_i \cos\theta_i, \tag{5}$$

$$F_L = \sum_{i=1}^{12} \left(p_i - p_{ref}\right) b_i \sin\theta_i, \tag{6}$$

where i is the tap number and θ_i is the arc angle of the i-th tap.

The reference pressure, p_{ref}, was measured far away from the location of cylinders. To minimize the potential influence of the downburst vortex on the measurements of static pressure, p_{ref} was chosen at the height of approximately 1.5 m above the floor. This height is above the top height of the leading downburst vortex. This selection of reference pressure is not typical for the classical wind engineering approach where p_{ref} is obtained at the height of the structure (Solari, 2019). This issue of the proper choice of p_{ref} in downburst outflows will be further discussed in section "Discussion of results and prospects for future research."

The reference velocities (U_{ref}) for the three investigated flows were measured at the height of pressure taps. In the DB and DBABL cases, U_{ref} is extracted as the peak velocity ($\hat{U}$) from the slowly varying mean velocity record:

$$\hat{U} = \max_{\forall t \in \Delta T} (\bar{U}(t)), \tag{7}$$

where t is the time, ΔT is the duration of the DB-like outflow, and $\bar{U}(t)$ is the slowly varying mean velocity. The moving mean averaging window was set at 0.05 s (Junayed et al., 2019; Romanic et al., 2019b). In the ABL wind case, U_{ref} is the mean ABL velocity at the height of the pressure taps (Solari, 2019). The reference velocity at the height of pressure taps is often used in the case of slender structures and elements.

Results

Flow field

The transient nature of the DB and DBABL outflows at the radial distance $r/D = 1.2$ from the undisturbed jet center is depicted in Figure 4(a) to (c). Both velocity records show the moving mean extracted from the instantaneous measurements at the height $z/L = 0.056$. In contrast to a stationary ABL wind, both DB-like outflows are characterized by a highly transient velocity ramp-up segment that is followed by the peak velocity around 1 s into the records. After reaching the peak, the velocity reduces to the quasi steady-state

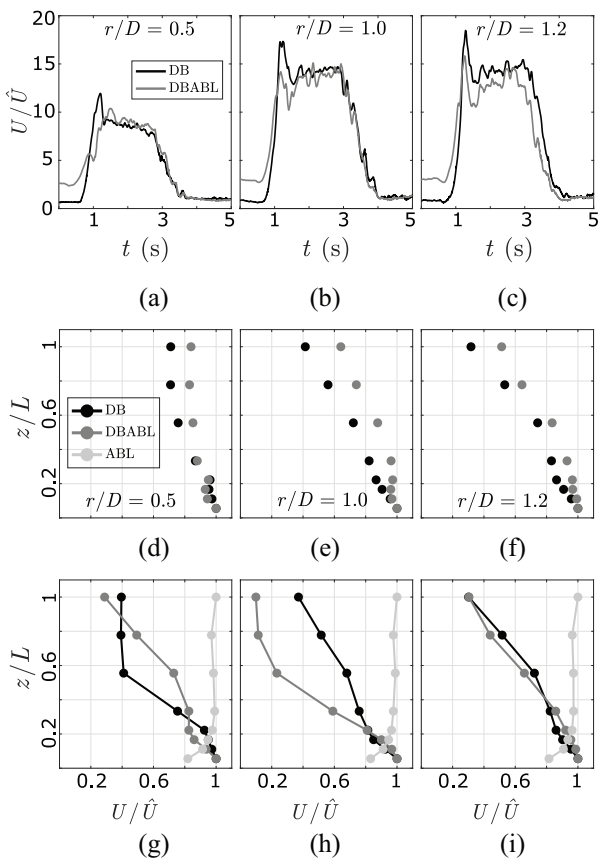

Figure 4. (a–c) Time histories of the ensemble mean velocities from multiple experiment repetitions at the height of $z/L = 0.056$ and three investigated r/D locations in the DB and DBABL outflows. (d–f) Normalized enveloped peak velocities at each height (i.e. the overall velocity peak at each height). (g–i) The vertical profile of velocities in the DB-like outflows at the time instant of velocity peak at $z/L = 0.056$. The ABL wind profile is also included in (g) to (i).

value that corresponds to the stationary impinging jet established after the passage of the primary vortex. The last portion of the velocity segments corresponds to the outflow dissipation caused by the termination of the DB-like downdraft. The DBABL velocities at the radial distance $r/D = 1.2$ are weaker than the DB winds (Figure 4(a)–(c)). However, the interplay between DB and ABL winds is complex and results in highly three-dimensional wind field in which the relative intensity between DB and DBABL winds highly depends on the position in the outflow. However, this subject will be addressed in detail in the upcoming studies.

The differences between the enveloped peak velocities in DB and DBABL outflows increase with the height (Figure 4(d)–(f)). The nose-shape curvature in the DBABL outflow is less pronounced than in the DB outflow. This result is in accordance with the numerical simulations in Mason et al. (2010) that demonstrate that the ABL wind tends to amplify the upper regions of the DBABL winds in this part of the outflow. Romanic and Hangan (2020) recently confirmed these findings experimentally. As stated earlier, the flow interaction is highly dependent on the investigated position in the flow field. Both DB-like cases profoundly differ from the logarithmic-like ABL wind profile.

The vertical profiles of radial wind speed extracted at the moment when the velocity peak is observed at the height $z/L \leqslant 0.056$ (Figure 4(d)–(f)) are significantly different from the enveloped velocity peaks at each height in Figure 4(d) to (f). The DB and DBABL outflows are stronger than the ABL winds at the heights below approximately $z/L = 0.1$. This result suggests that the DB-like winds are more dangerous to low-rise structures than high-rise buildings. The observed difference between either of the two DB-like profiles and the ABL wind profile also supports the observation discussed in the "Introduction" that the transmission lines—being a low-rise structure—are more prone to downburst than ABL wind failures.

Drag and lift coefficients

Overall, the ABL winds cause higher drag coefficients (c_D's) than the two DB-like outflows on the C040 cylinder (Figure 5(a)–(c)). The peak c_Ds in the DBABL outflow are slightly higher than in the ABL wind only close to the top of the cylinder at $r/D = 0.5$. However, the results shown in Figure 5(d) to (f) are more relevant for the wind loading investigations because of the c_D profiles of the DB-like outflows being extracted at the time of the peak c_D at $z/L = 0.056$. Thus, the profiles are time-dependent and represent the drag values that the structure experienced at that moment. While the mean c_D along the cylinders' height in the ABL winds is about 1.0 for both cylinders (slightly higher for C040), the c_D values in the DB-like outflows are strongly dependent on the height. At $r/D = 0.5$, the values close to the base of the cylinders are five to six times higher than at the top of the structures. While the height dependency of c_Ds at the other two radial locations in the DB-like outflows is not as pronounced as at $r/D = 0.5$, it is still larger than in the ABL winds. The c_D profiles in the DB-like outflows at $r/D = 1.0$ and 1.2 are similar, as expected. The largest discrepancies between the temporally enveloped peaks in Figure 5(a) to (c) and the time-dependent profiles of c_Ds in Figure 5(d) and (e) are at $r/D = 0.5$. These results indicate that the maximum c_Ds in the downdraft stagnation region (depicted later in Figure 12) are more challenging to analytically represent than they are in the wall region. In the wall region (Figure 12), the temporally enveloped peak c_Ds are similar to the c_D profile at the given moment in time (i.e. the time of the peak c_D close to the cylinders' base shown in Figure 5(d)–(f)). This similarity is not warranted in the stagnation region. Therefore,

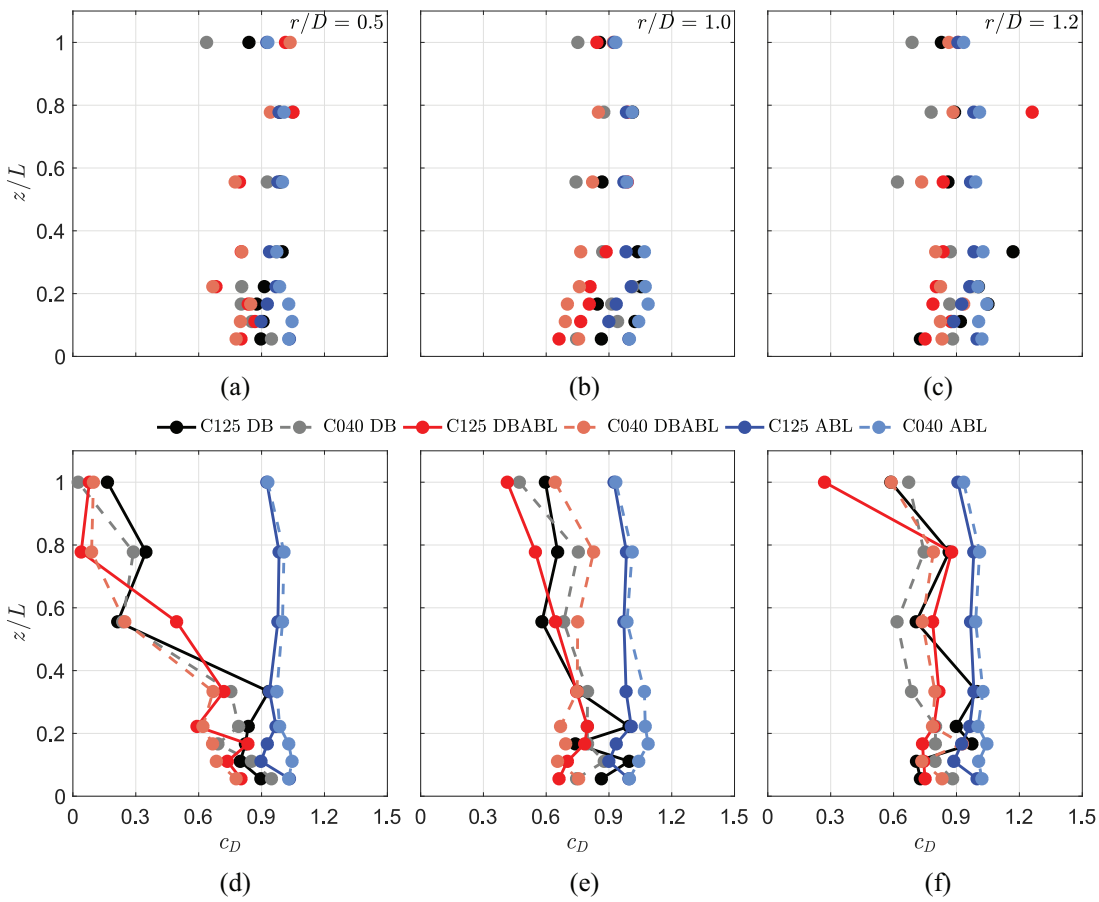

Figure 5. Drag coefficient (c_D) with height in the DB and DBABL outflows. The top row (a-c) shows the peak c_D at each height (i.e. the enveloped peak of c_D), while the bottom row (d-f) shows the vertical profile of c_D at the instant of peak c_D occurring at $z/L = 0.056$. The vertical profile of mean c_D in the stationary ABL wind is also shown. Cylinders location: (a, d) r/D = 0.5; (b, e) r/D = 1.0; and (c, f) r/D = 1.2.

the temporally enveloped peak c_Ds in the stagnation region might be too conservative for the practical implementation in design standards. These findings agree with the numerical study of Mason et al. (2009) that showed the loading of an isolated structure due to downburst winds never exceeded that from an ABL wind with an equivalent 10 m wind speed. However, our results indicate that the assumption of equal c_Ds in DB and ABL winds employed in Mason et al. (2010) might not be justifiable in the case of circular cylinders.

The c_D overshoot (Figure 6) for the two cylinders is defined as the ratio of the temporally enveloped peak c_D in the two DB-like outflows and the mean c_D of the steady ABL wind. This definition is adopted from Takeuchi and Maeda (2013), who analyzed the properties of non-stationary wind forces caused by a rapid wind gust on an elliptic cylinder. Interestingly, the c_D overshoot is overall below unity for C040, and the steady ABL winds tend to cause higher drag than the DB-like outflows. By comparing DB to DBABL values, the c_D overshoot is usually higher in DB outflow at lower elevations and vice versa (or similar values) close to the top of the cylinders. At $r/D = 1.0$ and 1.2, the c_D overshoot of DB outflow on the C125 cylinder is consistently higher than unity in the height interval $z/L = 0.1$ to 0.4. At the same time, the c_D overshoot of DBABL outflow is below unity. When benchmarked to the steady ABL winds, this result demonstrates that the inclusion of ABL winds in the DB simulations profoundly impacts the aerodynamics behavior of low-rise structures in the wall region of the DB-like outflows. For the C040 cylinder, both DB outflows feature the overshoot below 1. The only exception is the region at the top of the cylinder at $r/D = 0.5$, where both overshoots are higher than 1.

The mean lift coefficient (c_L) values in the ABL winds are around zero, as expected (Figure 7). The similarity between temporally enveloped peak c_Ls at $r/D = 0.5$ (Figure 7(a)) and the time-dependent c_L profile (Figure 7(d)) is much higher than in the case of c_Ds (Figure 5(a) and (d)). However, the most interesting result might be the sign of c_Ls in the DB-like winds.

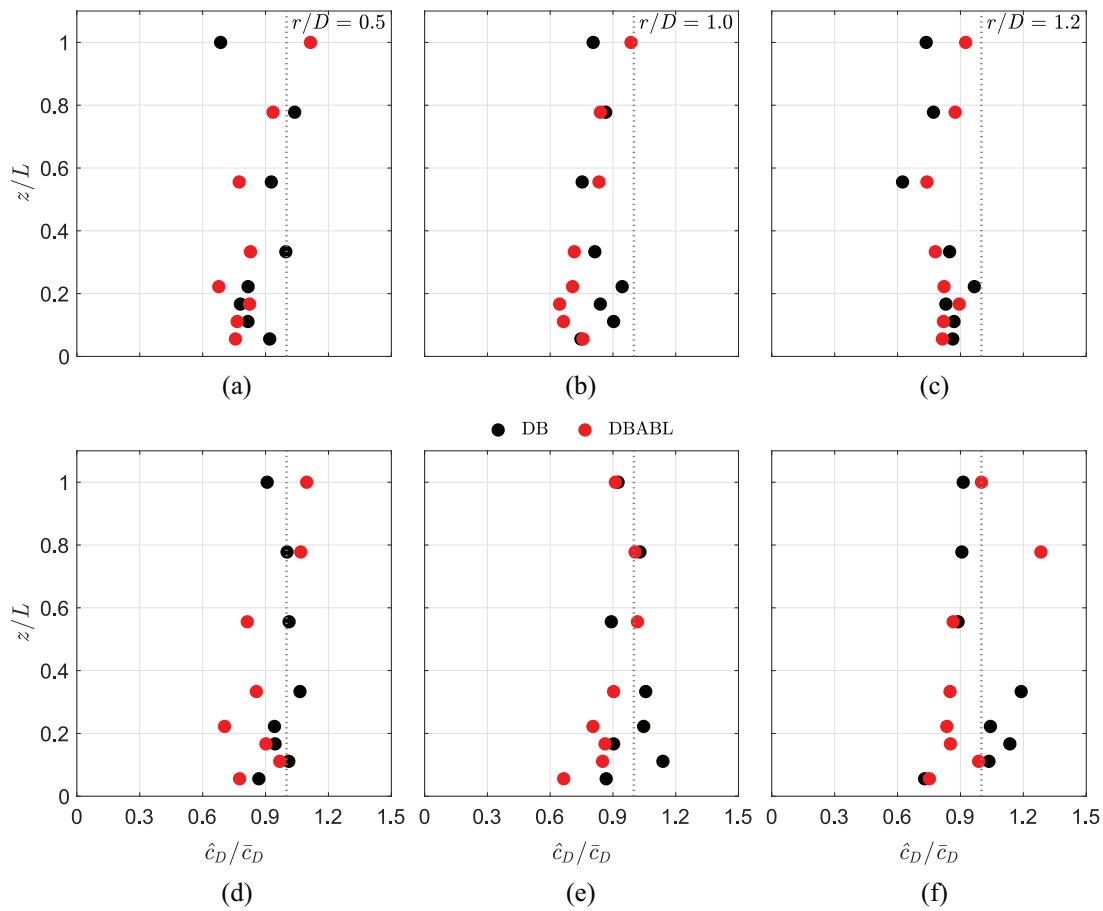

Figure 6. Drag coefficient (c_D) overshoot for the two DB-like outflows and C040 (a–c) and C125 (d–f) cylinders. The vertical dotted line is the c_D overshoot equal to 1. Each column represents one *r/D* position in the outflow (values shown in the top right of a-c).

Namely, the c_L values at the base of the cylinders are as low as -0.28 and rise to the slightly positive values or close to zero at the top of the structures. This trend is observed at all radial locations in the DB-like outflows, as well as in temporally enveloped peak c_Ls and time-dependent profiles. The result indicates that the DB winds might cause more complex dynamical behavior in the crosswind direction than ABL winds. This phenomenon of the change of the sign of c_L along the cylinders' height was also observed by Omori et al. (2008) in their large eddy simulations of sheared flows past a circular cylinder. The change in c_L sign from negative to positive occurs when the inviscid effects on the c_Ls become dominant over the wake effects (Omori et al., 2008). The trends of c_D and c_L profiles with height observed in this study corroborate well with the open fluid dynamics literature that demonstrated the c_L increases and the c_D decreases with increasing shear in the flow (Cao et al., 2007).

The c_D records close to the base and the top of the cylinders are markedly different from each other in the DBABL outflow (Figures 8 and 9). Discrepancies between the time signature of c_Ds in DB and DBABL outflows are observed close to the surface, while the time series show similar trends at the higher elevations. While the c_Ds are a non-stationary process in all cases, the absence of the dominant c_D peak in the DBABL outflow is readily observed at $z/L = 0.111$. This peak is associated with the passage of the primary vortex that translates radially outwards. These results demonstrate that the time evolution of the aerodynamics—while being weaker than that in ABL winds—is more challenging to model and more sensitive to the height.

Overall, the c_Ds around the smaller cylinder (C040) are slightly lower than around the larger cylinder (C125) at $z/L = 0.111$. Besides, we observe that the fluctuations of c_Ds are higher in the DBABL than in the DB outflow. The magnitudes of c_D fluctuations around C125 and C040 cylinders are similar. All differences are attenuated at a higher elevation (Figure 9).

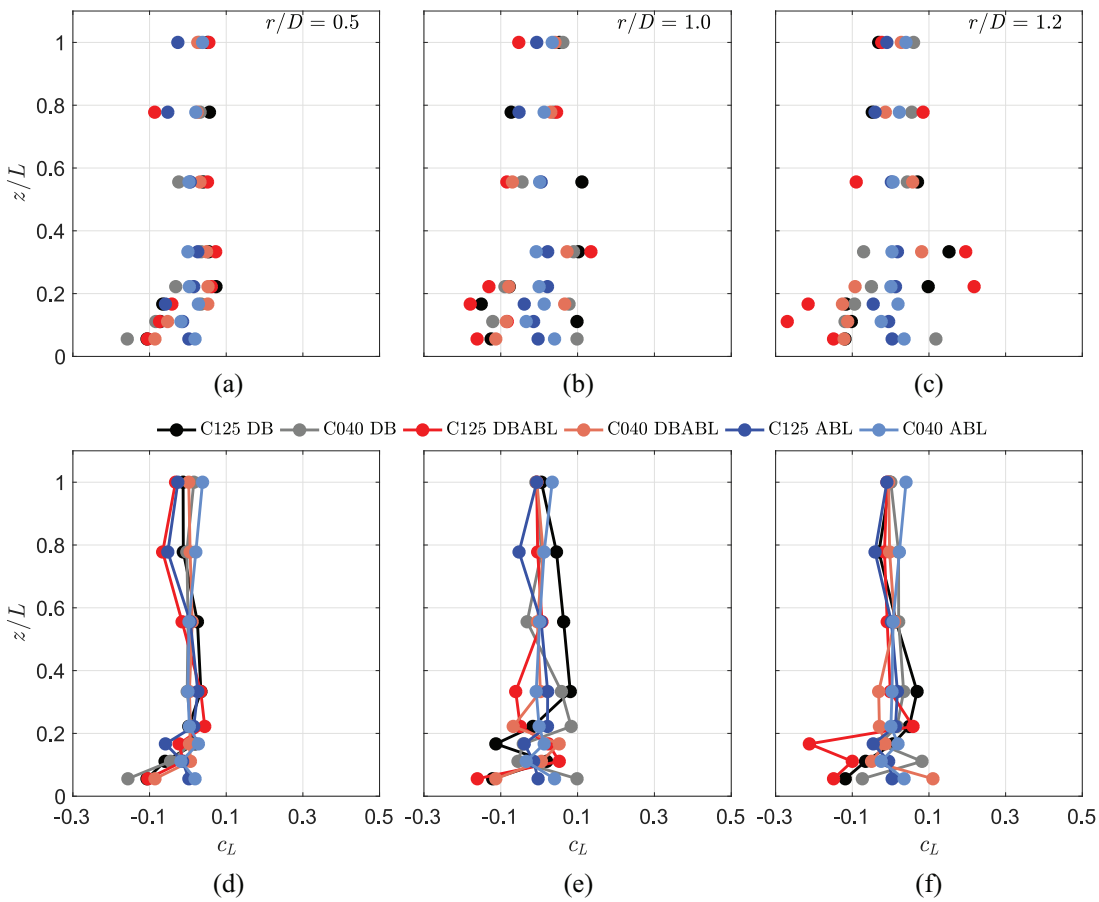

Figure 7. The top row (a-c) shows the peak lift coefficint (c_L) at each height (i.e. the enveloped peak of c_L), while the bottom row (d-f) shows the vertical profile of c_L at the instant of peak c_L occurring at z/L = 0.056. The vertical profile of mean c_L in the stationary ABL wind is also shown. Cylinders location: (a,d) r/D = 0.5; (b,e) r/D = 1.0; and (c,f) r/D = 1.2.

Surface pressures

The strong suction in the leeward side (tap #7) of both cylinders (Figures 10 and 11) is aerodynamically caused by the wake region behind the cylinders. While the surface pressures for the windward and leeward taps at $r/D = 1.0$ and $r/D = 1.2$ are fairly symmetric around zero value in the DB case; the symmetry line is shifted toward the positive value that corresponds to the ABL wind pressures in the DBABL cases.

We further notice that the surface pressures in the leeward side of the cylinders are slightly positive even during the ABL wind segment of the velocity record. This observation is caused by the "atypical" choice of reference pressure in the downburst outflows (section "Experiments setup and methodology"). This issue of proposing the proper location of the reference pressure measurements in DB-like outflows is still under investigation, and more discussion on this topic is included in section "Discussion of results and prospects for future research" (also see Jubayer et al., 2019). However, the primary significance of the pressure results presented herein is in their relative differences between different cases (DB versus DBABL) and not in the absolute values of the surface pressures obtained in any given experiment. For instance, the surface pressures at tap #7 are always lower than at tap #1 in the ABL portion of the DBABL velocity records (Figures 10 and 11).

The pressure distribution at $r/D = 0.5$ is profoundly different from that at the other two r/Ds. The symmetry between positive and negative pressures at tap #1 and tap #7 that is found at larger r/Ds is entirely lost at $r/D = 0.5$. At $r/D = 0.5$, both sides of the cylinders are characterized by positive surface pressures (Figures 10 and 11). Therefore, the notion of windward and leeward sides of the cylinders is not entirely justified in this situation. Also, the other 10 pressure taps on both cylinders are characterized by positive pressures (not shown) at this radial location in the outflows. The positive sign of surface pressures along the cylinders is due to the predominantly downward orientation of the DB and DBABL flows at $r/D = 0.5$. Here, the cylinders are close to or inside the downdraft region and the dominant component in the outflow is not radial, but rather the vertical (downward) velocity. Geometrically,

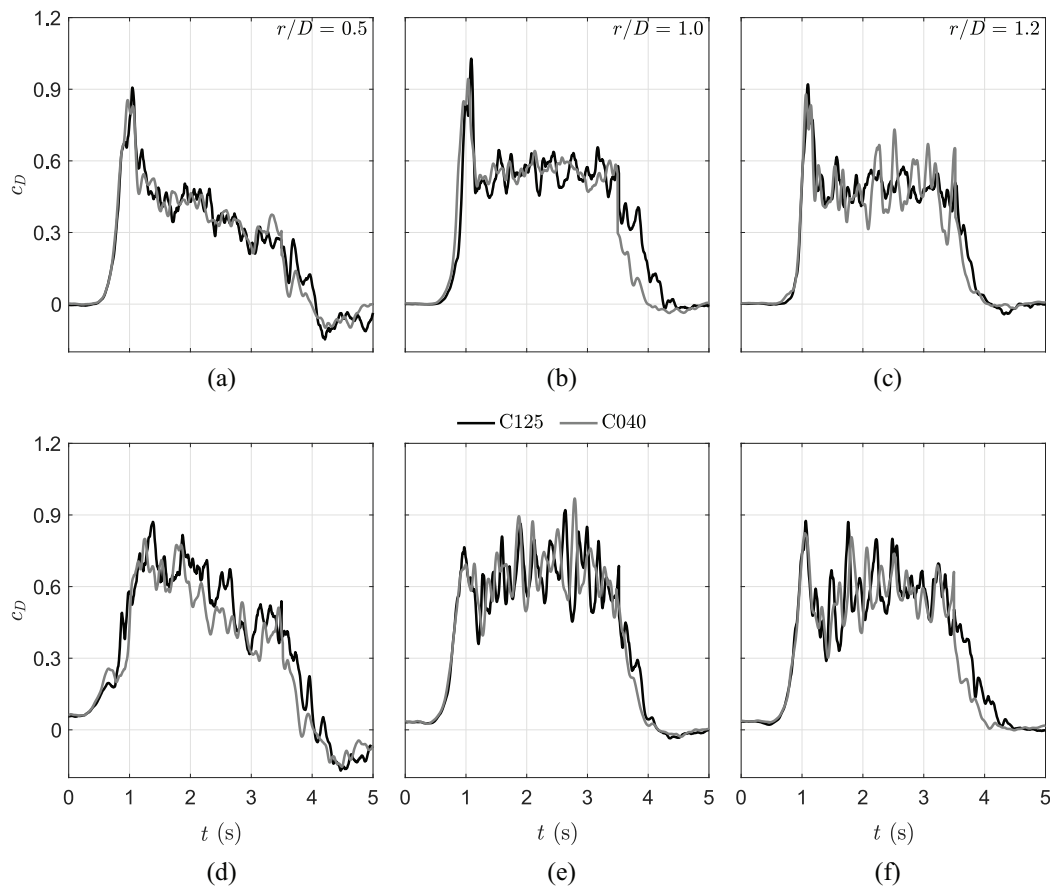

Figure 8. Time histories of drag coefficient (c_D) at the height $z/L = 0.111$ in the DB (a-c) and DBABL (d-f). The black and gray lines correspond to the C125 and C040 cylinders, respectively Cylinders location: (a, d) r/D = 0.5; (b, e) r/D = 1.0; and (c, f) r/D = 1.2.

$r/D = 0.5$ is at downdraft edge but effectively this location is inside the downdraft due to the widening of the downdraft after exiting from the bell mouth. The entrainment of the surrounding air into the impinging jet results in the loss of jet's momentum (Gauntner et al., 1970). This process is further accompanied by the loss of kinetic energy and the expansion of the velocity profile in the radial direction (Figure 12). However, the entire flow field is additionally altered in the DBABL case, which deserves further kinematic investigation in a separate study (Romanic and Hangan, 2020).

Figure 12 schematically demonstrates that all sides of the cylinders are similarly impacted by the downdraft at $r/D = 0.5$. Here, we say "similarly" because the windward side is still characterized by higher pressures than the leeward side, but there are no negative pressures in the leeward taps (Figures 10 and 11). We further notice from these figures that the relative difference between the pressures at different heights and at $r/D = 0.5$ is smaller than that at the other two radial positions. Once again, this difference is due to the underdeveloped radial outflow at $r/D = 0.5$ and the smaller nose-shape curvature of velocity profile at this location (Figure 12).

Discussion of results and prospects for future research

First, we comment on the free end and aspect ratio (AR) effects in our experiments. Okamoto and Yagita (1973) showed that the free end of cantilevered circular cylinders produces three-dimensionality of the flow around the cylinder and creates strong longitudinal trailing vortices in the tip region of the body. The same study, as well as Farivar (1981), demonstrated that the free end suppresses the periodic vortex shedding in the tip region. For short cantilevered cylinders with aspect ratio, $AR < 7$, this obstruction of vortex shedding propagates to the root of the cylinder. These experimental findings were later extended by Fox and West (1993a, 1993b), who demonstrated that the free end effects disappear after approximately 20 d from the tip. Their studies investigated cantilevered circular cylinders with AR in the range 4 to 30. Beyond 20 d, the flow conditions are the same as in the case of an infinitely long circular cylinder. Moreover, their results apply to a low-turbulent uniform flow at a Reynolds number of 4.4×10^4. As demonstrated later in this section, our

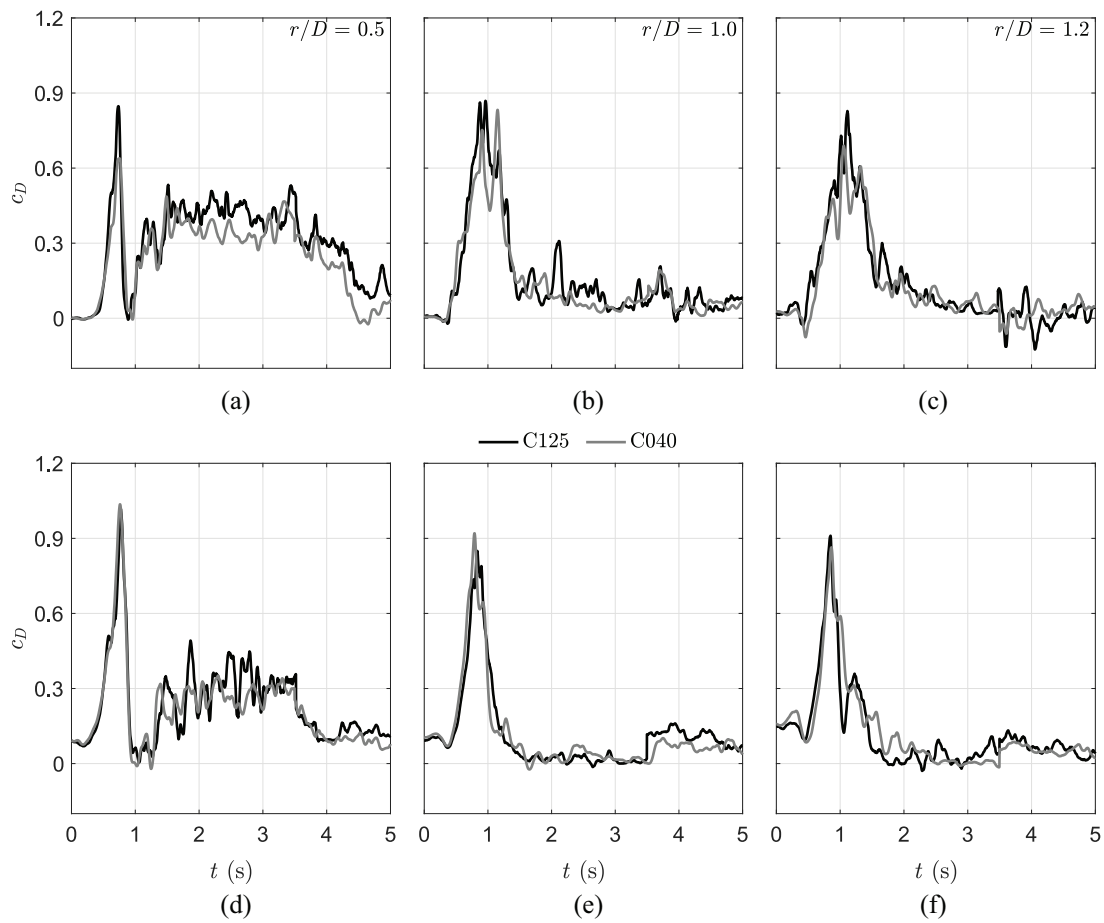

Figure 9. Time histories of drag coefficient (c_D) at the height z/L=1 in the DB (a-c) and DBABL (d-f). The black and gray lines correspond to the C125 and C040 cylinders, respectively. Cylinders location: (a,d) r/D = 0.5; (b,e) r/D = 1.0; and (c,f) r/D = 1.2.

experiments are characterized by a similar range of Reynolds numbers. Fox and West (1993b) also reported that the downwash significantly diminishes below 7 d from the free edge, leading to the increase of C_ps with moving away from the tip. With the taps being 10 d away from the free end in the current experiments, the results from Fox and West (1993b) indicate that the three-dimensionality effects reduce the c_Ds up to approximately 25% from those found along an infinitely long circular cylinder. The downwash effects are negligible. However, it is also important to highlight that their results apply to uniform flow, whereas the DB-like flow fields in this study are highly non-uniform. For instance, at $r/D = 1.0$ and $r/D = 1.2$, the DB-like flows have a strong upward component (Figure 1(b)) when impinging on the windward face in the top sections of the cylinders. This outflow does not promote any downwash regardless of the distance from the free end and AR. On the other hand, at $r/D = 0.5$, the DB-like outflows are predominantly downward (Figures 1(b) and 12) and, in fact, the entire cylinders are immersed into a downwash-like flow. Therefore, we propose more fundamental and experimental research contributions on bluff body aerodynamics in non-uniform and time-dependent DB-like outflows.

Secondly, the choice of the proper reference pressure and velocity in transient flows, such as downbursts and tornadoes, is still an open question in wind engineering society. The absence of a unified theoretical framework for referencing these flows results in different experimental procedures of replicating transient wind loading from one wind simulator to another, as well as from one type of DB-like outflows to another. Here, we used the peak velocity in the slowly varying velocity record at the height of pressure taps as the proper reference velocity in both DB and DBABL outflows. In principle, the reference velocity height could either be the characteristic height of the structure or the height of the maximum streamwise velocity in the outflow (Figure 12). The proper choice of reference pressure is also a nontrivial task. Two-dimensionality of the undisturbed ABL winds and the independence of static pressure in the streamwise direction of

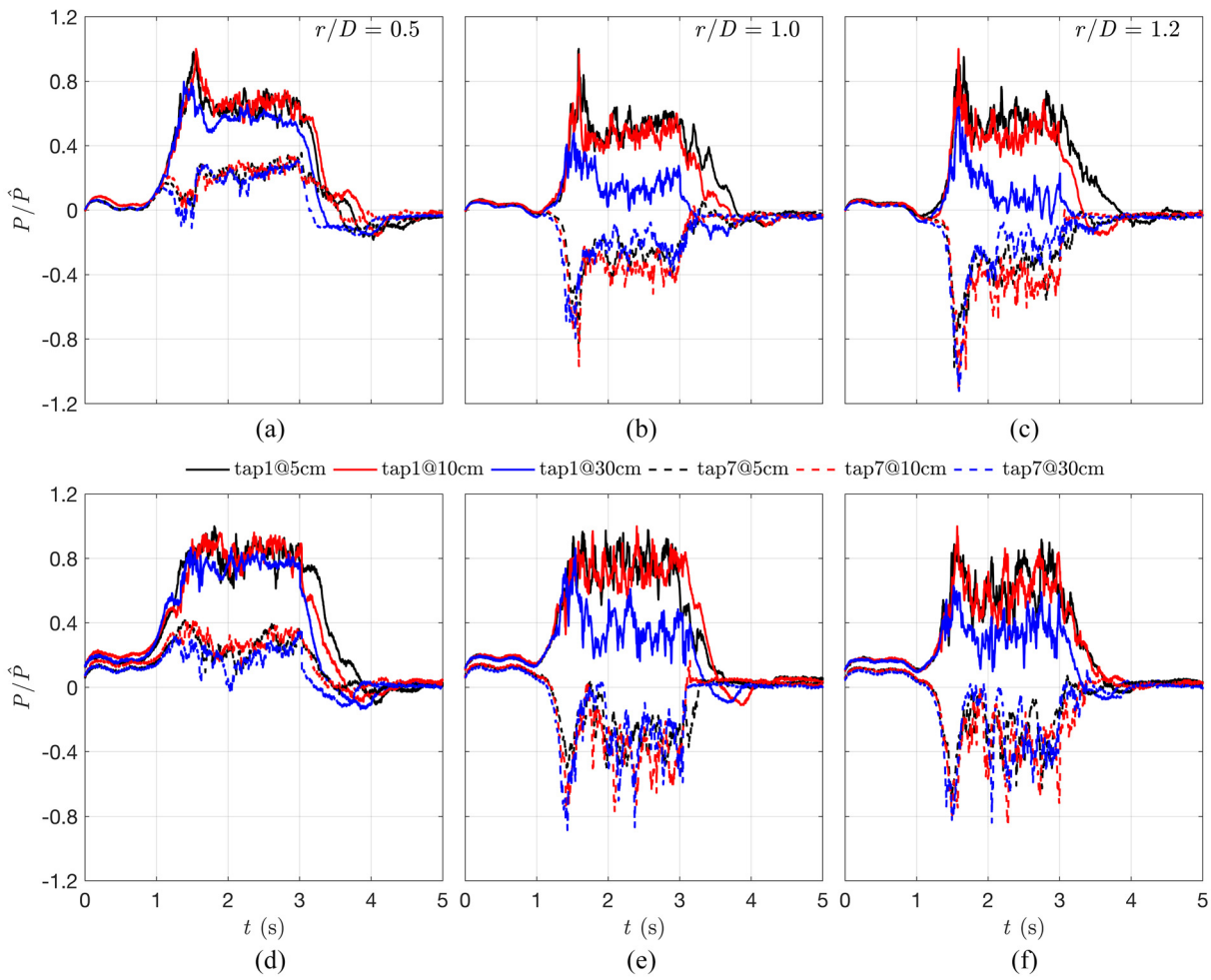

Figure 10. Time histories of normalized surface pressures at tap #1 (windward tap on the cylinders) and tap #7 (leeward tap on the cylinders) on the C125 cylinder. The top row (a-c) is for the DB outflow and the bottom row (d-f) for DBABL outflow. Cylinders location: (a, d) r/D = 0.5; (b, e) r/D = 1.0; and (c, f) r/D = 1.2.

developed ABL flow simplifies the choice of reference pressure in the standard engineering practice of testing structures to ABL winds. However, because DB-like outflows are naturally developing in all three spatial dimensions as well as time, this spatiotemporal transiency makes it rather difficult to pinpoint the representative location for reference pressure measurements in the DB-like outflows. This study measured the reference pressure at a location above the vortex height but inside the testing chamber. This choice of reference pressure, however, altered the values of ABL wind pressures from the values expected in the straight ABL winds (Figures 10 and 11). This discrepancy between the proper referencing for ABL and DB-like winds only demonstrates that more research is needed on relating physical simulations of downbursts to real events. For these reasons, we emphasized in section "Results" that the primary significance of the presented pressure results is in the relative comparisons between DB, DBABL, and ABL cases, and not necessarily in the absolute values of pressures.

This research focuses on circular cylinders in which cases the flow features are highly susceptible to the value of Reynolds number (Re). Here, Re is calculated using the cylinders' diameter (d) and the characteristic flow velocities (U_{ref}, provided in Table 2 for DB-like outflows and 3.3 m s^{-1} for the ABL wind, respectively) as:

$$Re = \frac{U_{ref} d}{\upsilon}, \tag{8}$$

where $\upsilon = 1.5 \times 10^{-5}$ m^2 s^{-1} is the kinematic viscosity of air.

The resulting values of Re in Table 3 show that the investigated flows are characterized by different Re depending on the cylinder and the flow in question.

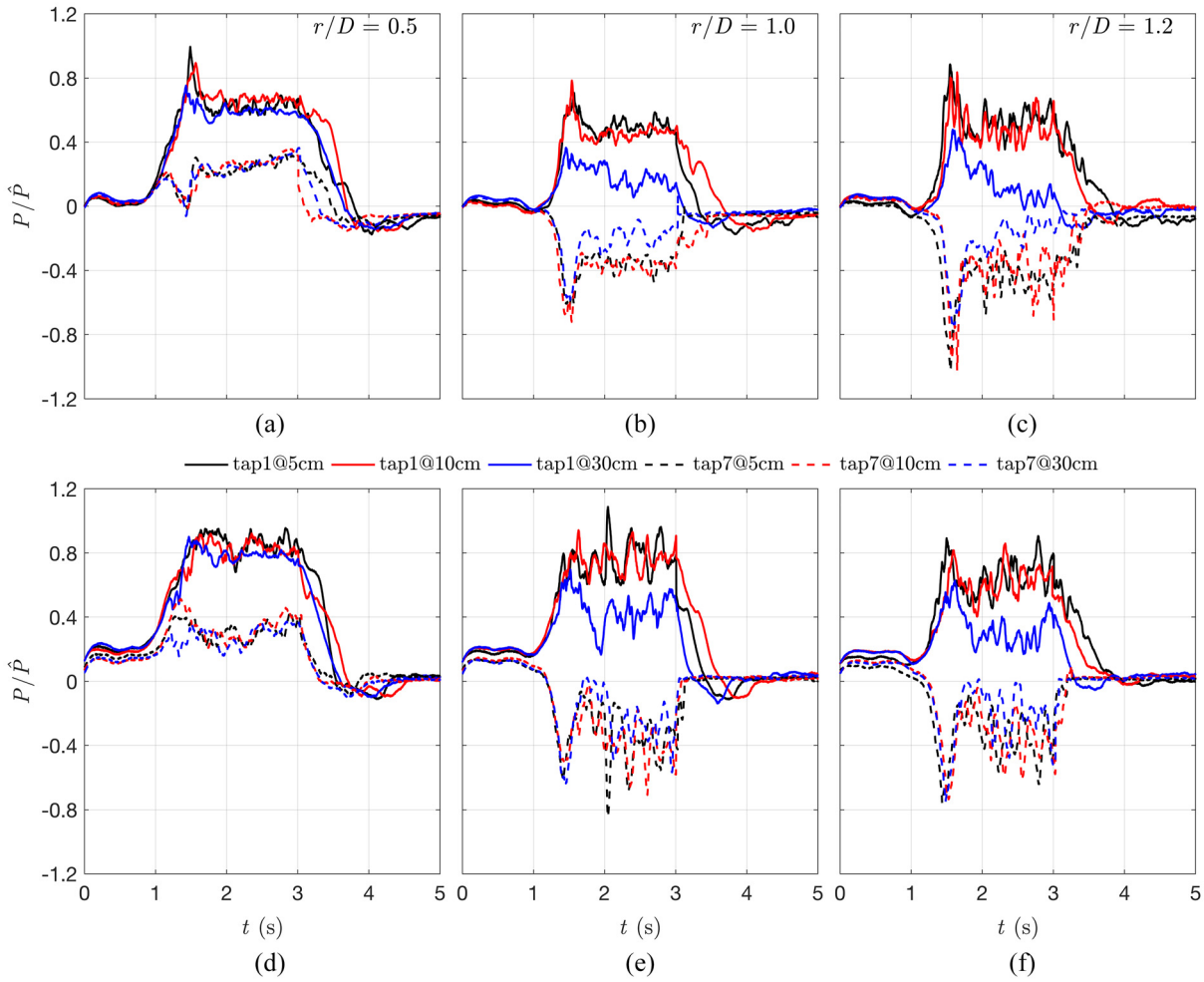

Figure 11. Time histories of normalized surface pressures at tap #1 (windward tap on the cylinders) and tap #7 (leeward tap on the cylinders) on the C040 cylinder. The top row (a-c) is for the DB outflow and the bottom row (d-f) for DBABL outflow. Cylinders location: (a,d) *r*/*D* = 0.5; (b,e) *r*/*D* = 1.0; and (c,f) *r*/*D* = 1.2.

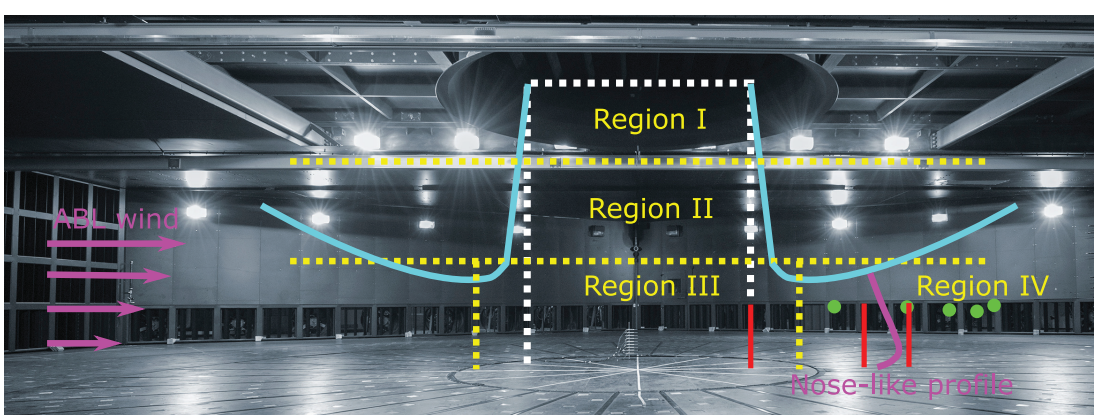

Figure 12. Schematics of cylinders' location (red sticks) in different outflow regions (yellow lines) of an impinging jet (cyan line): potential core region (I), free-jet region (II), stagnation region (III), and wall jet region (IV). The shape of the ABL wind profile and the nose-like profile of DB-like outflows in the wall jet region (IV) also shown (magenta lines). The dotted white line shows the initial diameter of the downdraft at the bell mouth. The green circles show the height of the primary vortex center in the analyzed DB outflow from the PIV measurements of Junayed et al. (2019).

Table 2. Peak velocities and their height at three radial locations in the two DB-like outflows.

	$\hat{U}$ (m s^{-1})			$\hat{z}$ (m)		
r/D	0.5	1.0	1.2	0.5	1.0	1.2
DB	11.93	17.33	18.47	0.05	0.05	0.05
DBABL	10.39	15.10	15.83	0.05	0.05	0.05

Table 3. *Re* values associate with three investigated flows and two circular cylinders.

Cylinder	DB	DBABL	ABL
C125	1.5×10^4	1.3×10^4	0.3×10^4
C040	4.9×10^3	4.2×10^3	0.9×10^3

The *Re* of ABL winds is lower than that of DB-like outflows. The C040 cylinder has an order of magnitude lower *Re* than C125 in the DB-like outflows, and approximately half of an order of magnitude lower *Re* in the ABL wind. However, c_D is weakly dependent on *Re* in the range presented in Table 3 (Potter et al., 2011). The *Re* values of 10^4 are similar to those analyzed by Fox and West (1993a, 1993b) in their study of cantilevered cylinders in a uniform turbulent flow. The range of *Re* in Table 3 is associated with a laminar vortex shedding flow in which the boundary layer around cylinders' surface is laminar, but alternative vortices are shed off the cylinders resulting in the von Kármán vortices. However, $Re = 10^4$ is also the borderline between the laminar vortex shedding and the subcritical turbulent flow regime in which the von Kármán vortices are becoming turbulent ($10^4 < Re < 2 \times 10^5$). Also, this study is restricted to smooth surfaces of the cylinders as well as the uniform surface roughness of the ground (bare floor). Moreover, the behavior of the DB-like outflows over the surfaces with abrupt changes of roughness, as well as their wind actions on the structures with rough body surfaces with non-uniform roughness are currently unexplored.

At a ~1:200 mean geometric scale of the WindEEE Dome downbursts (Romanic et al., 2019b), the diameters of C040 and C125 cylinders correspond to full-scale structures with the diameter of 0.8 and 2.5 m, respectively. The former diameter is similar to the luminary poles usually installed along the highways, whereas the latter diameter is in the range of wind turbine towers and chimneys. The maximum height of the tested cylinders reached 180 m above ground at the full-scale equivalent.

Lastly, a topic that deserves further research is the coupling between the transient velocity and aerodynamic behavior of structures. Recently, this subject was investigated by Mason and Yuanlung (2019) by analyzing the transient aerodynamics of the CAARC (Commonwealth Advisory Aeronautical Council) building in non-stationary velocity profiles. However, like the present work, the velocity and pressure measurements in their study were also desynchronized. The proper approach to investigate this aerodynamic dependency is through the convolution ($*$) integral:

$$(U * p)(t) = \int_0^t U(\tau)p(t-\tau)d\tau. \tag{9}$$

The blending of velocity (U) and pressure (p) signatures over the time interval (t) is only meaningful if the acquisition of two signals is synchronized. While the current study provided the general relationship between U and p in terms of the governing features of the DB-like outflows (e.g. ramp-up, primary vortex, ramp-down, nose-shape velocity profile), it was impossible to rigorously derive the lag (τ), if any, between U and p, and consequently U and c_D or c_L due to the desynchronization of these measurements. Recently, the importance of the $U - p$ lag was also demonstrated by Lombardo et al. (2018) in their full-scale measurements of downburst loading on a low-rise building. Their study applied a 2-s lag between the responses of surface pressures on the Texas Tech WERFL building and the velocity measurements on a nearby mast.

Conclusion

This experimental study analyzed the surface pressures and aerodynamic coefficients on two circular cylinders with free end immersed in three different wind fields. The diameters of these two cylinders were 12.5 mm (C125) and 4 mm (C040). The investigated flow fields were (1) a downburst outflow (DB), (2) a downburst outflow supplemented by atmospheric boundary layer (ABL) winds (DBABL), and (3) the steady ABL wind. The motivation to conduct this research came from the continually increasing wind engineering interest to better quantify the wind effects of non-synoptic winds, such as thunderstorm downbursts, on various structures. Circular cylinders—being the classical bluff body that was most studied in the classical fluid mechanics literature—was, therefore, also the starting point of

this research. The study provided the first comparisons between surface pressures and aerodynamic coefficients that resulted from these three different wind systems. The flow fields of experimentally produced DB and DBABL outflows were also examined. The main contributions are summarized below.

- The ABL winds caused a higher drag coefficient (c_D) than the two DB-like outflows on the C040 cylinder. The results are more height-dependent in the case of the C125 cylinder. The c_D overshoot—defined as the ratio of the peak c_D in the DB-like outflow and the mean c_D in the ABL wind—was higher in DB than in DBABL wind at the lower elevations and vice versa (or similar values) close to the top of the cylinders. At $r/D = 1.0$ and 1.2, the c_D overshoot in the DB outflow around the C125 cylinder was consistently higher than one between $z/L = 0.1$, and 0.4. Also, the c_D overshoot in the DBABL outflow in the same height interval was below unity. Therefore, the inclusion of ABL winds in the DB simulations significantly influenced the aerodynamics of low-rise structures in the outer regions of the DB-like outflows.
- The lift coefficients (c_Ls) during the passage of the primary DB-like vortex were negative at the base of the cylinders and approached zero or slightly positive values close to the cylinders' top. The change in a c_L sign was previously observed in high-shear flows in which there is a strong interplay between the inviscid and the wake effects on a cylinder's aerodynamics. In the study of ABL winds, the mean c_Ls are effectively zero.
- The location of the cylinders in the DB-like outflows is aerodynamically more significant than the diameter of a cylinder. This finding is profoundly different from the case of stationary ABL winds.
- While the surface pressures for the windward and leeward taps at $r/D = 1.0$ and $r/D = 1.2$ were symmetric around zero in the DB case; the symmetry line was shifted toward the positive value of the ABL wind pressures in the DBABL outflow. The pressure distribution at $r/D = 0.5$ was profoundly different from that at the other two radial locations. The symmetry between positive and negative pressures at tap #1 (windward tap) and tap #7 (leeward tap in the wake region) that was observed at larger r/Ds was gone at $r/D = 0.5$. The positive surface pressures everywhere around the cylinders at $r/D = 0.5$ were due to the predominantly downward orientation of the DB and DBABL outflows at this location. The traditional notation of windward and leeward sides of a structure is not meaningful in the regions close to the downburst center.
- Lastly, the study discussed various prospects for future experimental research in this field, such as the proper choices of pressure and velocity references in downburst outflows, and the velocity-pressure coupling that requires the synchronized measurements of these two quantities. Several uncertainties and underlining experimental assumptions were also critically discussed.

Acknowledgements

The authors thank Mr Hiroaki Shoji for his help with the experiments set up and MATLAB® coding. The authors also thank Prof. Massimiliano Burlando for his help with handling the Open Access publishing of this work. Lastly, the authors thank two anonymous reviewers for their comments that improved the quality of this work.

Declaration of conflicting interests

The author(s) declared no potential conflicts of interest with respect to the research, authorship, and/or publication of this article.

Funding

The author(s) disclosed receipt of the following financial support for the research, authorship, and/or publication of this article: The first, third and fourth authors acknowledge the support of the European Research Council (ERC) under the European Union's Horizon 2020 research and innovation program (grant agreement no. 741273) for the project THUNDERR – Detection, simulation, modelling and loading of thunderstorm outflows to design wind-safer and cost-efficient structures – awarded with an Advanced Grant 2016. The second author acknowledges the support of the Italian Ministry of Education, University and Research (MIUR) "Fondo Giovani" grant. The first and last authors acknowledge the support of the Canada Foundation for Innovation (CFI) WindEEE Dome Grant (no. X2281B38).

ORCID iDs

Djordje Romanic https://orcid.org/0000-0002-5935-807X
Federico Canepa https://orcid.org/0000-0003-0838-9930

References

Cao S, Ozono S, Hirano K, et al. (2007) Vortex shedding and aerodynamic forces on a circular cylinder in linear shear flow at subcritical Reynolds number. *Journal of Fluids and Structures* 23(5): 703–714.

Chay MT, Albermani F and Wilson R (2006) Numerical and analytical simulation of downburst wind loads. *Engineering Structures* 28(2): 240–254.

Chen L and Letchford CW (2004) A deterministic–stochastic hybrid model of downbursts and its impact on a cantilevered structure. *Engineering Structures* 26(5): 619–629.

Darwish MM and Damatty AAE (2011) Behavior of self supported transmission line towers under stationary downburst loading. *Wind and Structures* 14(5): 481–498.

Darwish MM, Damatty AAE and Hangan H (2010) Dynamic characteristics of transmission line conductors and behaviour under turbulent downburst loading. *Wind and Structures* 13(4): 327–346.

De Gaetano P, Repetto MP, Repetto T, et al. (2014) Separation and classification of extreme wind events from anemometric records. *Journal of Wind Engineering and Industrial Aerodynamics* 126: 132–143.

Elawady A, Aboshosha H and Damatty AE (2018) Aeroelastic response of transmission line system subjected to downburst wind: validation of numerical model using experimental data. *Wind and Structures* 27(2): 71–88.

Elawady A, Aboshosha H, El Damatty A, et al. (2017) Aeroelastic testing of multi-spanned transmission line subjected to downbursts. *Journal of Wind Engineering and Industrial Aerodynamics* 169(Suppl. C): 194–216.

ESDU (2002) *Characteristics of Atmospheric Turbulence Near the Ground. Part 2: Single Point Data for Strong Winds (Neutral Atmosphere). 85020*. London: ESDU International PLC. Available at: https://www.esdu.com/cgi-bin/ps.pl?sess = unlicensed_1170202220306nvc&t = doc&p = esdu_83045c-r1 (accessed 2 February 2017).

Farivar D (1981) Turbulent uniform flow around cylinders of finite length. *AIAA Journal* 19(3): 275–281.

Fox TA and West GS (1993a) Fluid-induced loading of cantilevered circular cylinders in a low-turbulence uniform flow. Part 1: mean loading with aspect ratios in the range 4 to 30. *Journal of Fluids and Structures* 7(1): 1–14.

Fox TA and West GS (1993b) Fluid-induced loading of cantilevered circular cylinders in a low-turbulence uniform flow. Part 2: fluctuating loads on a cantilever of aspect ratio 30. *Journal of Fluids and Structures* 7(1): 15–28.

Gauntner JW, Hrycak P and Livingood JNB (1970) Survey of literature on flow characteristics of a single turbulent jet impinging on a flat plate. NASA-TN-D-5652, E-5203. Technical report, NASA Lewis Research Center, Cleveland, OH, 1 February. Available at: https://ntrs.nasa.Gov/search.jsp?R = 19700009658 (accessed 17 February 2020).

Hangan H, Refan M, Jubayer C, et al. (2017) Novel techniques in wind engineering. *Journal of Wind Engineering and Industrial Aerodynamics* 171: 12–33.

Hangan H, Romanic D and Jubayer C (2019) Three-dimensional, non-stationary and non-Gaussian (3D-NS-NG) wind fields and their implications to wind–structure interaction problems. *Journal of Fluids and Structures* 91: 102583.

Hjelmfelt MR (1988) Structure and life cycle of microburst outflows observed in Colorado. *Journal of Applied Meteorology* 27(8): 900–927.

Ibrahim AM, El Damatty AA and El Ansary AM (2017) Finite element modelling of pre-stressed concrete poles under downbursts and tornadoes. *Engineering Structures* 153: 370–382.

Jubayer C, Romanic D and Hangan H (2019) Aerodynamic loading of a typical low-rise building for an experimental stationary and non-Gaussian impinging jet. *Wind and Structures* 28(5): 315–329.

Junayed C, Jubayer C, Parvu D, et al. (2019) Flow field dynamics of large-scale experimentally produced downburst flows. *Journal of Wind Engineering and Industrial Aerodynamics* 188: 61–79.

Kim J, Hangan H and Ho TCE (2007) Downburst versus boundary layer induced wind loads for tall buildings. *Wind and Structures* 10(5): 481–494.

Lombardo FT, Mason MS and de Alba AZ (2018) Investigation of a downburst loading event on a full-scale low-rise building. *Journal of Wind Engineering and Industrial Aerodynamics* 182: 272–285.

Markowski PM (2002) Hook echoes and rear-flank downdrafts: a review. *Monthly Weather Review* 130(4): 852–876.

Mason MS, Fletcher DF and Wood GS (2010) Numerical simulation of idealised three-dimensional downburst wind fields. *Engineering Structures* 32(11): 3558–3570.

Mason MS, Wood GS and Fletcher DF (2009) Numerical simulation of downburst winds. *Journal of Wind Engineering and Industrial Aerodynamics* 97(11–12): 523–539.

Mason MS and Yuanlung L (2019) Wind loading of the CAARC building during velocity profile transitions, part 1: transient pressure coefficient distributions. In: *The 15th international conference on wind engineering (ICWE15)*, Beijing, 6 September. Beijing, China: International Association for Wind Engineering (IAWE).

Nguyen CH, Freda A, Solari G, et al. (2015a) Aeroelastic instability and wind-excited response of complex lighting poles and antenna masts. *Engineering Structures* 85: 264–276.

Nguyen CH, Freda A, Solari G, et al. (2015b) Experimental investigation of the aeroelastic behavior of a complex prismatic element. *Wind and Structures* 20(5): 683–699.

Okamoto T and Yagita M (1973) The experimental investigation on the flow past a circular cylinder of finite length placed normal to the plane surface in a uniform stream. *Bulletin of JSME* 16(95): 805–814.

Omori T, Jakirlić S, Tropea C, et al. (2008) Shearless and sheared flow past a circular cylinder: comparative analysis by means of LES. *International Journal of Heat and Fluid Flow* 29(3): 703–720.

Potter MC, Wiggert DC and Ramadan BH (2011) *Mechanics of Fluids*. Boston, MA: Cengage Learning.

Qu W, Song W, Xia Y, et al. (2013) Two-step method for instability damage detection in tower body of transmission structures. *Advances in Structural Engineering* 16(1): 219–232.

Romanic D and Hangan H (2020) Experimental investigation of the interaction between near-surface atmospheric boundary layer winds and downburst outflows. *Journal of Wind Engineering and Industrial Aerodynamics* 205: 104323.

Romanic D, LoTufo J and Hangan H (2019a) Transient behavior in impinging jets in crossflow with application to downburst flows. *Journal of Wind Engineering and Industrial Aerodynamics* 184: 209–227.

Romanic D, Nicolini E, Hangan H, et al. (2019b) A novel approach to scaling experimentally produced downburst-like impinging jet outflows. *Journal of Wind Engineering and Industrial Aerodynamics*. Epub ahead of print January. DOI: 10.1016/j.jweia.2019.104025.

Savory E, Parke GAR, Zeinoddini M, et al. (2001) Modelling of tornado and microburst-induced wind loading and failure of a lattice transmission tower. *Engineering Structures* 23(4): 365–375.

Shehata AY and Damatty AAE (2007) Behaviour of guyed transmission line structures under downburst wind loading. *Wind and Structures* 10(3): 249–268.

Shehata AY, El Damatty AA and Savory E (2005) Finite element modeling of transmission line under downburst wind loading. *Finite Elements in Analysis and Design* 42(1): 71–89.

Solari G (2016) Thunderstorm response spectrum technique: theory and applications. *Engineering Structures* 108: 28–46.

Solari G (2019) *Wind Science and Engineering: Origins, Developments, Fundamentals and Advancements*. 1st ed. Springer tracts in civil engineering. Basel: Springer International Publishing.

Takeuchi T and Maeda J (2013) Unsteady wind force on an elliptic cylinder subjected to a short-rise-time gust from steady flow. *Journal of Wind Engineering and Industrial Aerodynamics* 122: 138–145.

Wang X, Lou W-J, Li H-N, et al. (2009) Wind-induced dynamic response of high-rise transmission tower under downburst wind load. *Journal of ZheJiang University (Engineering Science)* 43(8): 1520–1525.